Journal of Engineering Science and Technology
Vol. 6, No. 2 (2011) 131 - 145

CHARACTERISATION OF MULTIPHASE FLUID-STRUCTURE INTERACTION USING NON-INTRUSIVE OPTICAL TECHNIQUES

N. LAD[1,*], A. AROUSSI[2], D. ADEBAYO[1], M. AL-ATABI[3]

[1]Thermal and fluid Engineering, University of Leicester, University Road, Leicester, UK
[2]Department of Mechanical and Industrial Engineering, Qatar University,
P.O. Box 2713, Doha, Qatar
[3]School of Engineering, Taylor's University, Taylor's Lakeside Campus,
No. 1 Jalan Taylor's, 47500, Subang Jaya, Selangor DE, Malaysia
*Corresponding Author: nl63@le.ac.uk

Abstract

The purpose of this study is to determine experimentally the effectiveness of passive drag reduction techniques (which involve adjusting surface geometry) within a chaotic multiphase flow system. To quantify the intrusion and disturbance caused, a liquid-air blast atomiser continuously discharges within a test section of air at atmospheric pressure, with a circular cylinder placed 25 cylinder diameters (250 mm) downstream of the nozzle. This cylinder is then replaced with other cylinders which have modified surface geometry. The data was obtained using Particle Image Velocimetry (PIV) and determines the fluid motion resulting from spray structure interaction of a liquid spray with a circular cylinder. Subtraction of non intruded spray images from intruded spray images at the same locations, using the time averaged analysis allows the direct comparison of the amount of disturbance each geometric variant has on the spray. Using this data alongside velocity profiles time averaged trends were compared. Drag reduction from V-shaped grooves provides the greatest disturbance reduction. This is due to the reduced shear stress around its cross section and the addition of small liquid eddies within each V-groove creates a gliding surface. These features proved to be most effective when monitoring drag reduction in multiphase flow-structure interaction.

Keywords: Drag reduction, PIV, Spray, Circular cylinder, Fluid structure interaction.

1. Introduction

The study of flow around a circular cylinder is an area of great interest due to its fundamental importance and its relevance in technical applications. The flow

Nomenclatures

D	Diameter of droplet or diameter of cylinder, mm
L	Length of circular cylinder, mm
h	Height of ribs, mm
$\dot{m}$	Mass flow rate, kg/m^3
Re	Reynolds number
r	Radius of droplet, mm
s	Spacing, mm
U	Relative velocity, m/s
W	Weber number
Z	Ohnesorge number

Greek Symbols

ν	Kinematic viscosity, m^2/s
ρ	Density, kg/m^3
σ	Surface tension, N/m^2

Subscripts

crit	Critical
D	Based on diameter
g	Gas
L	Liquid
max	Maximum

Abbreviations

CFD	Computational fluid dynamics
PIV	Particle image velocimetry

characteristics have been investigated in the past by authors such as Roshko [1]. Hinze [2] and Schlichting [3] provide a review of the earlier works. In all of these studies, the upstream flow was both single phase and assumed uniform in approach profiles. For very small Reynolds numbers the wake consists of a steady recirculation region behind the cylinder. A description of an instability in the wake which was localised at a Reynolds number of Re = 25 was provided by [4]. A von Karman vortex street was first found to appear at an approximate Reynolds number of Re = 49 [5]. At a critical Reynolds number of $Re_{crit} \approx 194$ the wake flow becomes three-dimensional. The first three-dimensional instability that appears is characterized by a spanwise wave-length of around 3*D*-4*D*, where *D* is the diameter of the cylinder. This is the result of an elliptic instability and it scales on the primary vortex structure, which is the larger structure in the flow. In the region of $Re_{crit} \approx 240$ the instability reduces in size in the spanwise wave-length by a factor of three. In the subcritical range where Re lies between 10^3 and 2×10^5, the flow around the cylinder is entirely laminar and transition happens in the free shear layer downstream of the cylinder. With increasing Reynolds number, the location of transition gradually moves upstream. For Reynolds numbers above Re = 2×10^5, the location of transition moves so far upstream that the boundary layer along the cylinder becomes partially turbulent. As a consequence, the boundary layer separation downstream is deferred thereby reducing the size of the

wake and, because of that, also the losses and increasing drag [6]. At Re = 3900, in the lower subcritical range, several experiments were performed by [7-11]. Details of these experiments are described in [11] and [12].

From the above review it has been recognised that the majority of previous works have been carried out within a controlled flow domain which has very little upstream turbulence. Previous studies usually involve single phase flows with the use of seeding particles for either measurements or visualisation. This study has been setup to investigate some of the developed passive flow control techniques which involve subtracting material from the original body to form channels. Since passive control techniques within uniform flows have been the main focus of research in previous years, this paper has extended the techniques to monitor the effectiveness of various designs within the complex multiphase flows of an atomised spray. Spray flow systems are complex due to the unpredictability of the liquid phase being transported.

This study is primarily focused on passive control techniques. These involve the modification of surface geometry or skin type to physically control the way in which the flow passes over the bluff body. To date these techniques have had extensive amounts of scrutiny. For example, parameters involving longitudinal grooves, riblets/micro riblets, rubber rings, wavy surfaces, aerofoils, splitter plates and devices to trip the flow have been investigated. These small modifications made to the surface of the bluff body (in this case a D=10 mm, L=150 mm circular cylinder) control the vortices produced within the downstream wake, usually by reducing the size of the vortices created and reducing the size of localised eddies.

The installation of riblets with longitudinal grooves on surfaces is well known as an effective flow control method that reduces drag [13]. The performance of grooved surfaces applied on bluff bodies has been known to depend largely on the surface configuration of adapted grooves. The investigated of the drag reduction achieved by installing longitudinal ribs on a flat surface for various rib shapes were carried out by Walsh [14]. It was observed that the drag reduction was associated with a decrease of momentum and turbulent velocity fluctuations, and depended primarily on the configuration of the ribs, determined by parameters such as the height (h), spacing (s) and shape. The study describes a maximum of 8% drag reduction for a symmetric V-groove surface of depth $h^+ < 25$ and spacing $s^+ < 30$ (h^+ and s^+ are dimensionless parameters in wall units). It was also concluded that the rib with sharp peaks is among the best rib shape for drag reduction. This phenomenon was also discovered by Bechert and Bartenwerfer [15]. They determined that the sharp ridges of the riblets impede cross-flow in the viscous sub-layer and that the presence of riblets decreases turbulent momentum exchange in the boundary layer, reducing the wall shear stress. The investigation by Choi [16] described the near-wall structure over smooth and grooved surfaces. The study found that the control of spanwise movement of longitudinal vortices was a key mechanism for drag reduction over riblet surfaces. A study by Choi et al. [17] used direct numerical simulations of the instantaneous turbulent structures over V-shaped riblets with $s^+ = 20$ and 40. For the drag increasing surface ($s^+ = 40$), streamwise vortices of about 30 wall units in diameter move freely inside the riblet valleys. However, at $s^+ = 20$, most of the streamwise vortices stay above the riblets, leading to drag reduction. Ko et al. [18] and Leung and Ko [19] investigated the effect of a V-groove configuration on the reduction of drag on a circular cylinder by measuring the surface pressure and Strouhal number

variations. The V-grooved and smooth cylinders showed nearly the same drag coefficient in the Reynolds number range from 2×10^4 to 1.6×10^5.

Lim and Lee [20] investigated the flow around circular cylinders with U- and V-shaped grooved surfaces by measuring the drag force, mean velocity and turbulence statistics of the wake. The U-shaped grooves were found to be more effective in drag reduction, compared with the V-shaped grooves. However, the detailed drag reduction mechanism and the modified three-dimensional flow structure around the U-grooved cylinders were not fully understood. Achenbach [21] and Guven et al. [22] mentioned that surface roughness on a circular cylinder influences the vortex shedding, drag coefficient and heat-transfer characteristics.

Spray characteristics

Sprays consist of two-phase (gas-liquid) flow in which the liquid phase is the dispersed phase and exists in the form of many droplets. The gas phase is the continuous phase in which the dispersed phase travels. The droplets and the gas have velocities that can be different, so both phases can move through some fixed volume or chamber and the droplets can move relative to the surrounding gas.

Sprays extend out to many areas, with practical applications in fields ranging from large power generating plants, to spray drying, paint spraying, crop protection, and a multitude of others. Previously these areas have had an active interest in research and development, making progress in the fields of Computational modelling of turbulent spray particle sizing. These areas have been quite distinct primarily with the introduction of new non intrusive imaging techniques. To date the majority of the research within the spray genre has been primarily on atomisation, spray structure and particle sizing. This is fuelled by the fact a small percentage in improvement to a number of spray characteristics i.e., in spray drying or combustion, can increase efficiency or more importantly reduce pollutant emissions.

Since the spray characteristics come in exhausting number, this study is limited to the specific investigation of air blast atomisation techniques. These types of sprays are utilised to apply uniform paints to car body panels, among other applications. Figure 1 describes the nozzle schematic typically used for air blast atomisation to produce droplet sizes of approximately 10-15 μm.

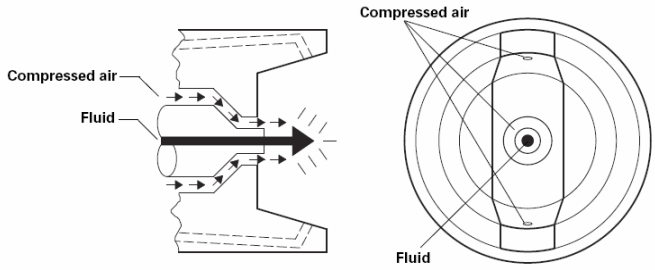

Fig. 1. Schematic Diagram of Nozzle Orifice for an Air Blast Atomiser.

Atomisation properties vary dramatically due to the characteristics of the dispersed spray phase and the secondary continuous phase and also the geometry of the mixing zone of the two phases. These phases are primarily characterised using: gas density, ρ_g, gas (kinematic) viscosity, v_g, liquid density, ρ_L, liquid viscosity, v_L, and liquid surface tension σ_L.

The characteristic of gas-liquid relative velocity ($U_g - U_L$) within the break up zone is important to recognise to state spray initial conditions. This relativity should consider swirl flow however, the spray device does not provide any swirl the swirl factor is neglected. Derivations of relationships between the relative velocities, geometrical properties of the atomiser and input initial conditions can be made by semi-empirical methods. These input conditions are: air and liquid mass flow rates, $\dot{m}_g$ and $\dot{m}_L$, and characteristic orifice dimensions. Heat transfer between the two phases during cold spraying is minimal and is neglected. The derivations from the above conditions produce non-dimensionless parameters. Primarily Reynolds numbers, Re, which can define the flow structure of the spray and Weber number, We, where Re is the measure of the relative importance of inertial forces and viscous forces and is calculated using Eq. (1). Reynolds number in this study is approximately 3500 and is calculated using air velocity at the nozzle orifice (0.8 mm). When considering a droplet or a ligament with a diameter D, We_D is defined in Eq. (2).

$$\mathrm{Re}_D = \frac{\Delta U D \rho_g}{\mu_g} \tag{1}$$

$$\mathrm{We}_D = \frac{\Delta U^2 D \rho_g}{\sigma_L} \tag{2}$$

Construction of a dimensionless group which describes the relative importance of viscous and surface tension forces within a sheet, ligament or droplet; is the viscosity group, or Ohnesorge number, Z, which, for a droplet, is defined as:

$$Z = \frac{\mu_L}{\sqrt{\sigma_L D \rho_L}} \tag{3}$$

We_D and Z values are important factors when investigating droplet break up models. For very low Weber numbers near the critical value of about 6 the droplet executes oscillation and may break up into two new droplets of equal size. For Weber numbers between 25 and 50 the droplets become a bag shape and as the Weber number increases the bag will allow stripping and forming secondary smaller droplets. As the Weber numbers exceeds 50 there is catastrophic droplet break up.

In this study the Weber number calculated around the nozzle orifice is approximately 12 and therefore it can be assumed that the atomised sprayer used will not perform any droplet break-up. This can therefore simplify CFD models, and increase the accuracy of PIV solutions obtained. Due to the complexity of sprays when modelling it is simpler to assume droplets as spherical shapes. This in-turn allows simpler methods of particle sizing techniques and allows computationally less demanding numerical techniques. Another assumption being made is that no vapour exists within the system before the nozzle inlet, and

therefore no vapour is produced within the entrainment of the spray. This would allow a simple mass balance between the liquid throughputs at the atomiser

$$\dot{m}_L = \int r(\dot{m}_L + \dot{m}_v) dr d\theta \tag{4}$$

For a full cone axisymmetrical spray the throughput mass balance is defined as:

$$\dot{m}_L = \int 2\pi r(\dot{m}_L + \dot{m}_v) r dr \tag{5}$$

where $r = D/2$.

A typical two phase flow originated from a pressure atomizer can be characterised into three different regimes. Directly at the nozzle orifice an intact core of liquid phase can be identified. This rapidly diminishes into ligaments (churning flow) and then further into droplets. These phase changes still occupy a significant fraction of the volume. The characteristics of individual droplets fluctuate throughout the spray. Interactions between droplets occur, such as, collisions and coalescence. This phenomenon occurs more often towards the nozzle orifice. As the spacing between droplets is reduced the boundary layer of the droplet is affected by the adjacent droplets.

2. Geometrical Setup

The identification of the geometry types under test within this study are outlined in Fig. 2. All bodies have receeding elements which aid in drag reduction and will be compared against that of a standard 10 mm circular cylinder of length 150 mm. Geometries have been decided upon by techniques which have been observed by previous authors as noted in Section 1. A range of each technique type has been produced to effectively monitor the drag reduction effectiveness of its own species of geometries as well as others. The various bodies have been code named as seen in Fig. 2, the circular cylinder is identified as "REF". For describing data obtained with no fluid-structure interaction, the term "NONE" is used.

This paper focuses on passive flow control techniques which involve subtracting material from the initial 10 mm diameter circular cylinder. The passive control types used also ensure that the drag reduction is not flow direction dependant.

3. Experimental Setup

In order to explore droplet transport around a circular cylinder, an experimental arrangement is used that provides a well-characterized homogeneous turbulent flow field around the obstacle. The experimental setup includes a non-swirling air that co-flows around the liquid injector. The experiment is oriented horizontally, as opposed to the original vertical arrangement, to prevent liquid droplets downstream of the obstacle from hitting a surface and falling back upstream into the oncoming stream. The agent used in this study was water that was supplied to the flow field with a 40° solid-cone pressure-jet atomizer with an air pressure of 410-450 kPa and a specified flow rate of 0.0045 kg/s. For these experiments, the incoming air (supplied from a 7 L/min compressor) was directly connected to the spray gun via a regulator valve. A Double pulsed laser was utilised to produce a sheet of laser

energy. A 4 Mpixel CCD camera with a 60 mm lens was used to focus upon the particles of seeder highlighted by the laser sheet. The seeder utilised is Sphericel 50 µm (Hollow Glass Spheres). The set up is described in Fig. 3.

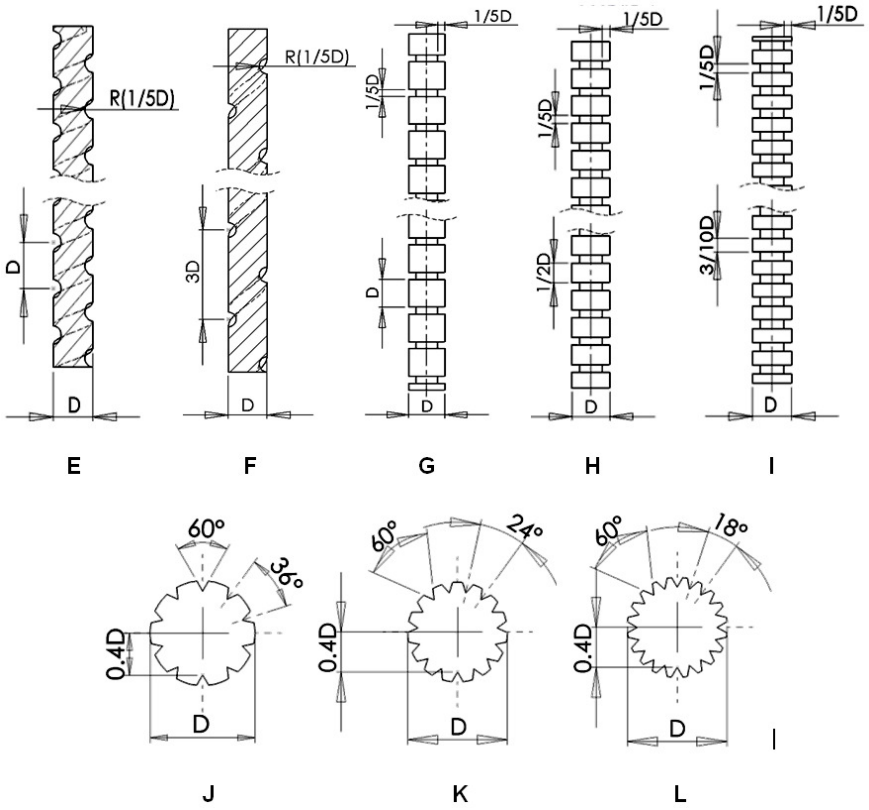

Fig. 2. Various Probe Geometries used within the Spray Flow Regime. Length is 150 mm for all Shapes. Shapes J, K and L are Uniform Cross Sections.

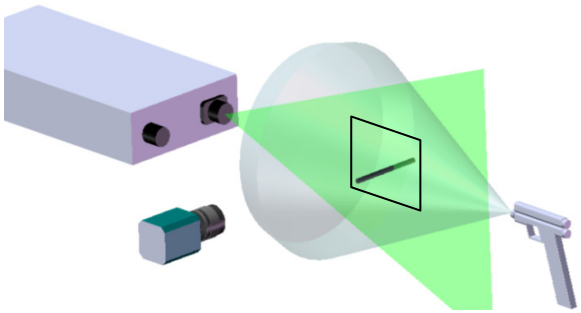

Fig. 3. Experimental Setup of Spray System for Analysis of Wake Properties by the Cylinder Cross Section.

The laser control, laser/camera's synchronisation and data acquisition and processing were handled by a hardware module and Dynamic Studio software

installed on a standard PC. The time interval between two laser pulses was equal to 15 μs which allowed approximately two to three diameters of particle movement between frames. The trigger rate of the camera was set to 4 Hz and approximately 150 images were captured in each run. This value was used due to the limitations of computational power when processing the images. The image area was located 250 mm downstream of the nozzle exit allowing a viewing window of 280 mm×300 mm. Recorded images were correlated using a 32×32 pixel interrogation area with 50% overlapping. Velocity patterns from PIV measurements are time dependant. Since the trigger rate of the camera was limited to 4 Hz it was too slow to pickup smooth transitions between image pairs for accurate time dependant analysis.

4. Results and Discussion

Subtraction of non intruded spray images from intruded spray images at the same locations. Using the time averaged analysis allows the direct comparison of the amount of disturbance the obstacle has on the spray. By subtraction of the 'NONE' data from any fluid-structure interaction data it is clear we obtain a magnitude plot of deviation (Fig. 4). From these images it is evident that a large area of a small deviation would suggest that the shape in question is effective at reducing the intrusiveness within the spray flow. This analysis is carried out for all shapes as shown in Fig. 5.

Using colour thresh-holding techniques, the percentage area of the image is calculated for bands of subtracted values i.e., the difference between the images. The results are observed in Table 1. Table 1 also breaks these areas down into velocity magnitude segments. Having an intruded image with a high amount of low velocity deviation and low amount of high velocity deviation suggests that the shape in question produces less intrusion.

All shapes are compared against a standard 10 mm circular cylinder which is described in Table 1 as "REF". In the higher range between 5-11 m/s deviation, the REF data only calculates approximately 5%. It is clear that much of the high velocity difference caused in this area is primarily due to the effect of the shape itself. A shape with a lesser cross section will have a lower amount of zero velocity and there for outlines a much smaller area of high velocity intrusion. This is obviously the case since shapes E to L have deviations from 5-11 m/s ranging only from 2.45% to 4.32%. The REF data shows approximately 80% of the image is 0-3 m/s deviation which suggests the image is very similar to that of un-intruded flow. By comparing this to all other shapes it is obvious that this result is worse than those of helical grooves of E, F, J, K and L and very similar to horizontal riblets of G, H and I.

It is evident that the vertical grooves within spray flows provide a more efficient drag reduction technique. This is due to the ability to trap fluid within the grooves. The build up of fluid and its eddy motion within them creates both a gliding boundary layer and a small amount of suction. Through analyses the cross flow over the vertical grooves reduces the amount of shear stress the flow is observed when passing around the grooved cross section. By increasing the number of grooves reduces the surface area of solid material exposed to the spray flow after the grooves are filled with trapped liquid.

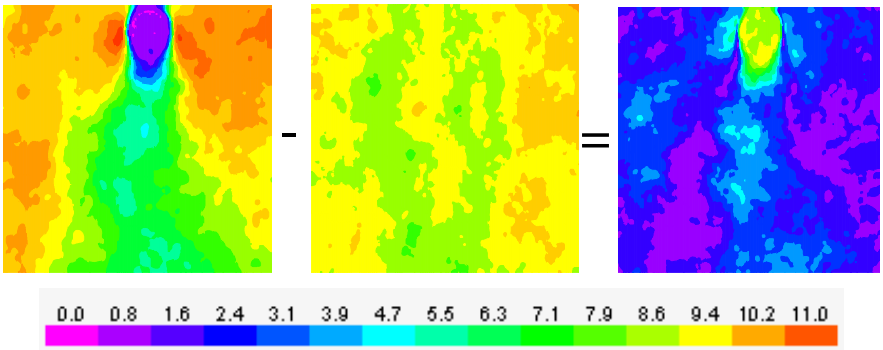

Fig. 4. PIV Image of the REF subtracted by NONE to create the Magnitude Plot of Deviation in m/s.

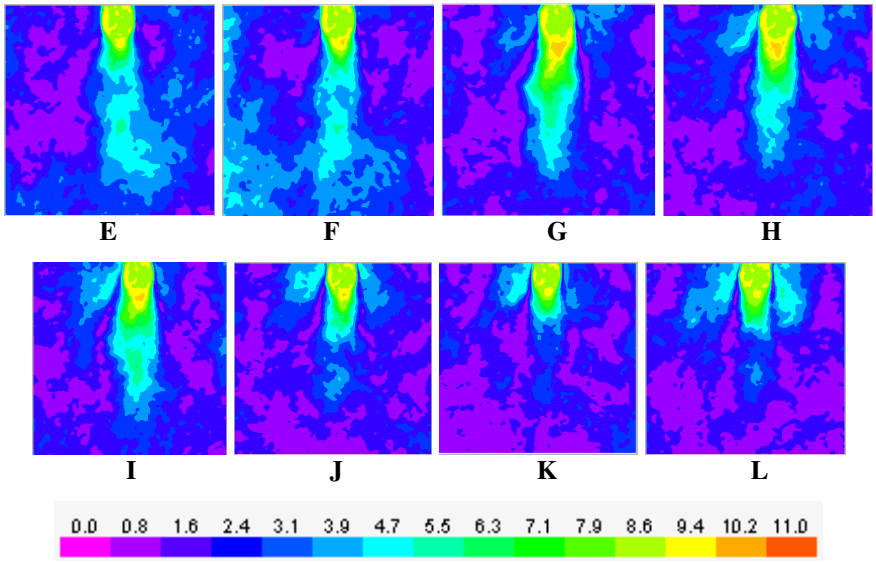

Fig. 5. In order from Top Row Left to Right. Probes E, F, G, H, I, J, K and L describe the Change in Velocity from the Spray without Intrusion. These Plots were achieved by $U_i - U_o$ (Velocity Magnitude of the Spray with Intrusion subtracted by the Spray with no Intrusion.

Through observation it is evident that the majority of the image area is between 0-3 m/s, this incorporates the lowest two possible velocity magnitude bands. By analysing this band of deviation it can be monitored which shape provides a consistently low deviation from that of non-intruded flow. The data is provided in Table 2.

It is believed that having a consistently low deviated image from that of the un-intruded flow the shape is deemed to have better near wake drag reduction qualities. Table 2 shows a slightly different trend to that of the analysis of 0-1 m/s

deviation. The REF data shows 81.3% of the image has a deviation of 0-3 m/s. It is evident that only E, F, and G (75.9%, 64.4% and 81.2% respectively) show a significant decrease in area for the same velocity deviation segment. This then suggests that utilising the horizontal riblets produces a flow regime which is worse than the reference shape when comparing with of non-intruded flow. Also to highlight the effectiveness of horizontal V shaped grooves the consistency of probes J, K and L are significantly better than that of the "REF" probe.

Using vector subtraction in this way to compare flow effects from different geometries provides an insight into direct numerical comparison from PIV images. It enables the user to clearly extract flow differences from time averaged PIV data. The technique does have some uncertainties when trying to understand the deviated flow regime. Since the subtraction of vectors is velocity magnitude only ($V^2=X^2+Y^2$) it is difficult to understand whether the flow 0-3 m/s slower or faster than that of the non-intruded flow regime. Using velocity magnitudes it is difficult to understand the actual flow property, which is why it is convenient to describe the flow differences between shapes using the "deviation" from non-intruded flow. Also since this technique is 2D PIV it omits the effects of velocity in the z-direction.

Table 1. Percentage Area of the Image with Respective Deviation from U_i-U_o.

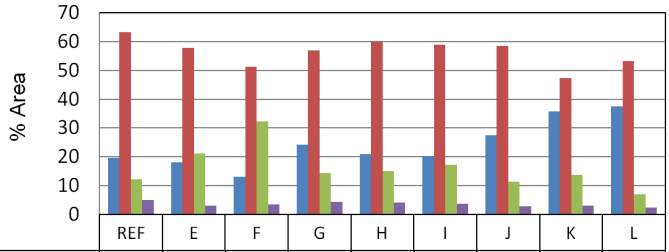

	REF	E	F	G	H	I	J	K	L
% Area of image showing 0-1m/s difference	19.61	18.18	13.05	24.22	20.93	20.28	27.44	35.86	37.53
% Area of image showing 1-3m/s difference	63.19	57.7	51.32	57.01	59.88	58.84	58.39	47.39	53.11
% Area of image showing 3-5m/s difference	12.24	21.1	32.23	14.45	14.99	17.21	11.29	13.74	6.91
% Area of image showing 5-11m/s difference	4.96	3.02	3.4	4.32	4.2	3.67	2.88	3.01	2.45

Table 2. % Area of Image showing 0-3 m/s Difference.

REF	E	F	G	H	I	J	K	L
81.29%	75.88%	64.37%	81.23%	80.81%	79.12%	85.83%	83.25%	90.64%

Velocity magnitude profiles were also obtained on non subtracted images to determine the flow structure downstream of the probe. This enables the observation of flow recovery and also quantifies the wake properties. The profiles where taken at 2, 3, 4 and 5D (where D = 10 mm) downstream of the shape. These velocity profiles were obtained using time averaged PIV solutions. 150

pairs of images were acquired at 4Hz per pair of images. This allowed a good accurate representation for accurate statistical averaging. The profiles were obtained using 2D PIV and therefore omit the velocity in the z-direction. Figure 7 describes the velocity profiles for all shape types. All velocity magnitudes have been normalised with respect to the flow at the spray nozzle orifice (U_{max}). Within uniform flow regimes these wake effects appear prominently at even 20*D* downstream. Atomised spray flow however is deemed to be an unsteady flow where the shear around droplets determines its direction. It is predicted that the wake within a spray recovers quicker due to the nature of spray flows as characterised in Section 3.

Better drag reduction techniques can be identified by the characteristics of the velocity profiles observed downstream of the bluff body. As the profiles move further downstream of the intruding body the losses associated with it diminish. Therefore the profiles become more uniform and the standard deviation of the profile curve reduces. The effectivity of the drag reduction shape is monitored by locating the most uniform profile downstream of the bluff body within five diameters.

The wake structure downstream of each shape variant is easily identified in Fig. 7. All profile plots are approximately symmetrical in nature suggesting the geometry variances do not force any one sided shear which will cause wakes similar to that of rotating bodies. Although this is the case shapes J, K and L shows at 5*D*, the flow shows very little momentum loss compared to other shapes. By carful observation the plots at both 4*D* and 5*D* are very similar. Shapes E, F, G, H and I all produce larger peak velocity values which are caused by excessive acceleration at the sides of the shape. This is due to a larger pressure drop. This is not observed in probes J, K and L as the grooves aid in reducing the pressure drop thus reducing the acceleration along the sides of the cross section.

By analysing the standard deviation of each profile plot the spread of the data can be determined. It is obvious that the optimal standard deviation is produced by the spray flow without any intrusion. From observation of Table 3 it is clear that shapes J, K and L show consistently better results for both in close proximity and further downstream standard deviation figures.

By studying the standard deviation of velocity profiles in Table 3 it is clear that most varieties of passive control techniques improve the flow recovery when compared to that of the circular cylinder. The standard deviation figures for NONE describe the ideal deviation for each profile downstream. For an efficient drag reduction technique the deviation should be as close to this as possible. It is obvious that that shapes J, K and L produce the most consistently low deviations. However the adjustments in geometry give slightly different results. By comparison against that of NONE, shape J has a greater standard deviation at 2*D* and 3*D*. However, further downstream, at 4*D* and 5*D*, the standard deviation is greatly reduced, to become similar to that of NONE. This is the opposite to probe L. The data trends suggest that as number of longitudinal grooves increase around the circumference of a circular cylinder, the effect of flow disturbance tends more towards the near wake region. By reducing the number of longitudinal grooves, the reduction of disturbances have proved to be further downstream. Through parametric study, came the creation of shape K, which is the median of all vertical groove techniques within this study. By observing Table 3, it is clear that

statistically probe K is more effective than J and L as it is effective at near wake and further downstream.

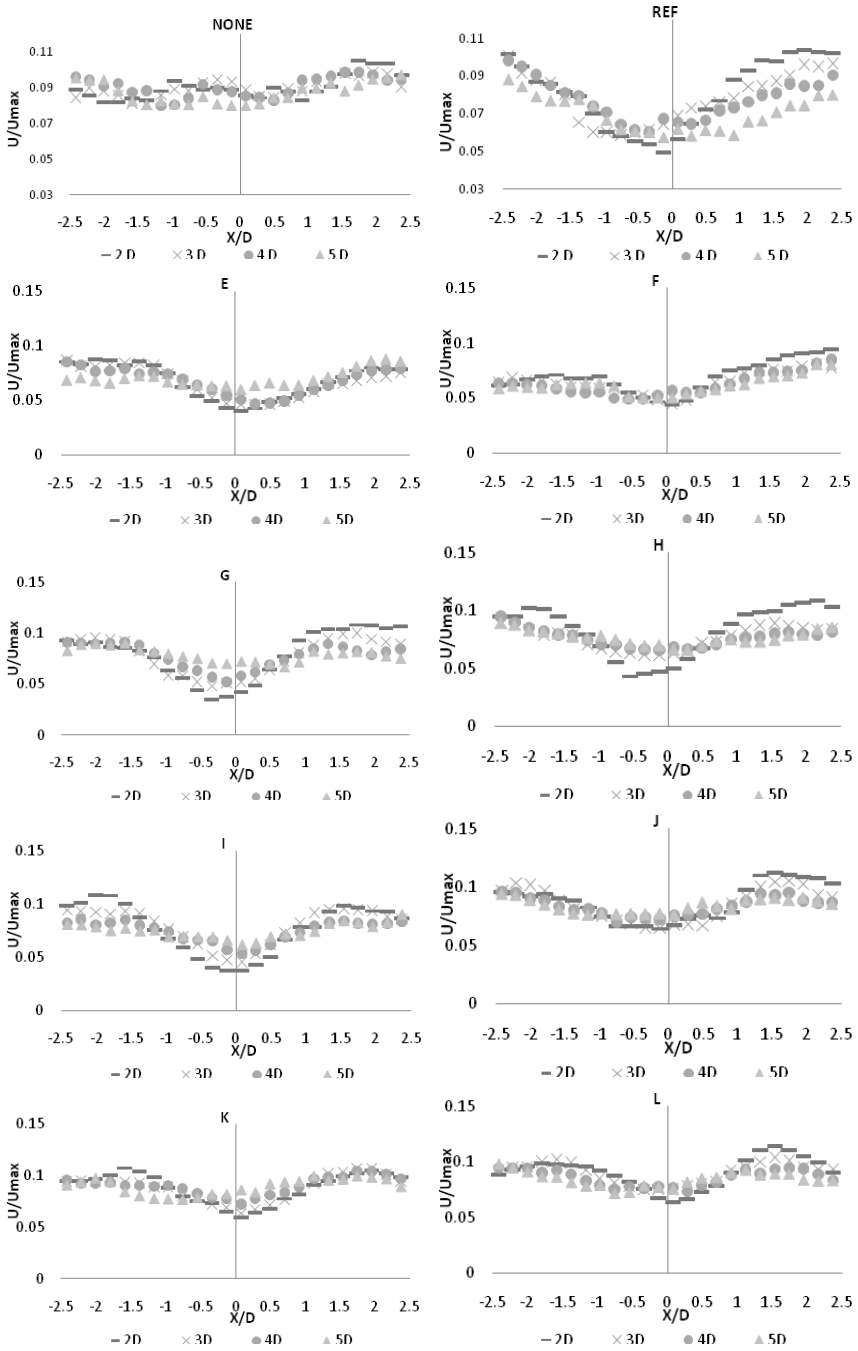

Fig. 7. 2D Velocity Profiles obtained at Various Diameters Downstream of the Shape Location.

Table 3. Standard Deviation of Profile Plots.

Name	2*D*	3*D*	4*D*	5*D*
NONE	0.0073	0.0051	0.0055	0.0061
REF	0.0186	0.0138	0.0120	0.0093
E	0.0130	0.0127	0.0106	0.0065
F	0.0108	0.0082	0.0084	0.0071
G	0.0161	0.0119	0.0086	0.0048
H	0.0140	0.0106	0.0118	0.0110
I	0.0168	0.0131	0.0078	0.0057
J	0.0107	0.0101	0.0069	0.0061
K	0.0090	0.0080	0.0064	0.0067
L	0.0090	0.0062	0.0075	0.0081

5. Conclusions

Within this study the effects of Fluid structure interaction within a multiphase spray flow were investigated experimentally using the non-intrusive optical technique (PIV). The Flow control techniques were all passive evolutions of a circular cylinder of 10 mm diameter and 150 mm in length. The techniques involved the forming of helical grooves, horizontal riblets and longitudinal V-shaped grooves. Each species of technique has small variations to create multiple structures to enable parametric studies. Two methods were used to observe the intrusiveness and interactivity of each probe type. The first being an analysis of the area density for contour values obtained by PIV, the second being a series of velocity magnitude profile plots from 1*D* to 5*D* downstream of the structure. It was observed that all passive control techniques decreased the flow intrusiveness compared to that of the circular cylinder.

It is clear that helical channels, case the flow to travel in the thread direction. This causes similar flow features to that of a rotating cylinder or a cylinder near a boundary. This is produced by the shear around the surface not being symmetrical in nature. From the study it is clear that the reduction in wake size was only minimal compared to that of the reference cylinder. It is obvious that horizontal riblets of shapes G, H and I showed conclusive evidence to prove a successful flow control technique. They proved to produce fewer disturbances than that of a circular cylinder. However when analysed against the longitudinal grooves they were substandard in comparison. This was due to the difference in the interactivity of structure and water droplets. Vertical grooves provide less shear stress around its cross section and the addition of small liquid eddies within each V shaped grooves help create a gliding surface. These features proved to be most effective when monitoring drag reduction in multiphase flow-structure interaction.

References

1. Roshko, A. (1954). On the development of turbulent wakes from vortex streets. *NACA Report 1191*, National Advisory Committee for Aeronautics.
2. Hinze, J.O. (1975). *Turbulence*. (2nd Ed.), McGraw Hill Inc., New York.
3. Schlichting, H. (1979). *Boundary-layer theory*. 7th Ed., McGraw Hill Inc., New York.
4. Monkewitz, P.A. (1988). The absolute and convective nature of instability in two-dimensional wakes at low Reynolds numbers. *Physics of Fluids*, 31(5), 999-1006.
5. Williamson, C.H.K. (1996). Vortex dynamics in the cylinder wake. *Annual Review of Fluid Mechanics*, 28, 477-539.
6. Wissink, J.G.; and Rodi, W. (2008). Numerical study of the near wake of a circular cylinder. *International journal of heat and fluid flow*, 29(4), 1060-1070.
7. Dong, S.; Karniadakis, G.E.; Ekmekci, A.; and Rockwell, D. (2006). A combined direct numerical simulation-particle image velocimetry study of the turbulent near wake. *Journal of Fluid Mechanics*, 569, 185-207.
8. Lourenco, L.M.; and Shih, C. (1993). Characteristics of the plane turbulence near wake of a circular cylinder, a particle image velocimetry study. Published in Beauden and Moin (1994). Data taken from Kravchenko and Moin (2000).
9. Norberg, C. (1994). An experimental investigation of flow around a circular cylinder: influence of aspect ratio. *Journal of Fluid Mechanics*, 258, 287-316.
10. Ong, L.; and Wallace, J. (1996). The velocity field of the turbulent very near wake of a circular cylinder. *Experiments in Fluids*, 20(6), 441-453.
11. Norberg, C. (2003). Fluctuating lift on a circular cylinder: review and new measurements. *Journal of Fluids and Structure*, 17(1), 57-96.
12. Varlamov, Y.D.; Meshcheryakov, Y.P.; and Predtechensky, M.R. (2008). Sequential absorption of microdrops by double-layer porous media. *Journal of Engineering Science and Technology (JESTEC)*, 3(3), 197-212.
13. Gad-el-Hak, M. (1989). Flow control. *Applied mechanics reviews*, 42(10), 261-293.
14. Walsh, M.J. (1983). Riblets as a viscous drag reduction technique. *AIAA Journal*, 21(4), 485-486.
15. Bechert, W.D.; and Bartenwerfer, M. (1989). The viscous flow on surfaces with longitudinal ribs. *Journal of Fluid Mechanics*, 206, 105-129.
16. Choi, K.S. (1989). Near-wall structure of a turbulent boundary layer with riblets. *Journal of Fluid Mechanics*, 208, 417-458.
17. Choi, H.; Moin, P.; and Kim, J. (1991). On the effect of riblets in fully-developed laminar channel flows. *Physics of Fluids A*, 3(8), 1892-1896.
18. Ko, N.W.M.; Leung, Y.C.; and Chen, J.J.J. (1987). Flow past V-groove circular cylinder. *AIAA Journal*, 25(6), 806-811.
19. Leung, Y.C.; and Ko, N.W.M. (1991). Near wall characteristics of flow over grooved circular cylinder. *Experiments in Fluids*, 10(6), 322-332.

20. Lim, H.C.; and Lee, S.J. (2002). Flow control of circular cylinders with riblet surfaces. *AIAA Journal*, 40(10), 1631-1642.
21. Achenbach, A. (1971). Influence of surface roughness on the crossflow around a circular cylinder. *Journal of Fluid Mechanics*, 46, 321-335.
22. Guven, O.; Farell, C.; and Patel, V.C. (1980). Surface roughness effects on the mean flow past circular cylinders. *Journal of Fluid Mechanics*, 98, 673-701.